Electronic Supplementary Material (ESI) for Green Chemistry.
This journal is © The Royal Society of Chemistry 2019

Electronic Supplementary Information to

Robust and Electron Deficient Oxidovanadium(IV) Porphyrin Catalysts for Selective Epoxidation and Oxidative Bromination Reactions in Aqueous Media.

Tawseef Ahmad Dar, Bhawna Uprety, Muniappan Sankar* and Mannar R. Maurya*

Department of Chemistry, Indian Institute of Technology Roorkee, Roorkee – 247667, India

Table of contents	**Page No**.
Figure S1. MALDI-TOF spectrum of **1** in CH_2Cl_2 using HABA matrix.	3
Figure S2. MALDI-TOF spectrum of **2** in CH_2Cl_2 using HABA matrix.	3
Figure S3. FT-IR spectra of (a) 3,5-dimethoxyphenyl porphyrin (b) **1** and (c) **2** using KBr pellets.	4,5
Figure S4. MALDI-TOF spectrum of oxidoperoxido species of **1** in CH_3CN generated with H_2O_2 and $NaHCO_3$ using HABA matrix.	5
Figure S5. MALDI-TOF spectrum of oxidoperoxido species of **2** in CH_3CN generated with H_2O_2 and $NaHCO_3$ using HABA matrix.	6
Figure S6. Thermogram (TG), Differential thermal analysis (DTA) and Differential thermogram (DTG) of 3,5-dimethoxyphenyl porphyrin, $H_2(TPP)(OMe)_8$ at a heating rate of 10 °C /minute scanned from 25 °C to 1000 °C.	6

Figure S7. Thermogram (TG), Differential thermal analysis (DTA) and Differential thermogram (DTG) of (**1**) at a heating rate of 10 °C /minute scanned from 25 °C to 1000 °C.	7
Figure S8. Thermogram (TG), Differential thermal analysis (DTA) and Differential thermogram (DTG) of (**2**) at a heating rate of 10 °C /minute scanned from 25 °C to 1000 °C.	7
Figure S9. B3LYP/LANL2DZ set generated optimized geometry of **1** showing (a) top view and (b) side view. In the side view, front and back side substituents are not shown for better viewing.	8
Figure S10. UV-Visible spectra of **1** and **2** after being recovered from the catalytic reactions in CH_2Cl_2 at 298 K.	9
Table S1. UV-Visible spectral data and molar absorptivity constants of **1** and **2** in CH_2Cl_2 at 298 K.	8
Table S2. Crystal structure data of VOTPP$(OMe)_8$ (**1**) and VOTPP$(OMe)_8(Br)_{16}$ (**2**).	9
Table S3. Selected average bond lengths and bond angles for VOTPP$(OMe)_8$ (**1**) and VOTPP$(OMe)_8(Br)_{16}$ (**2**) from single crystal XRD studies.	10
Equation 1: Equation used for calculating TOF (h^{-1}).	10

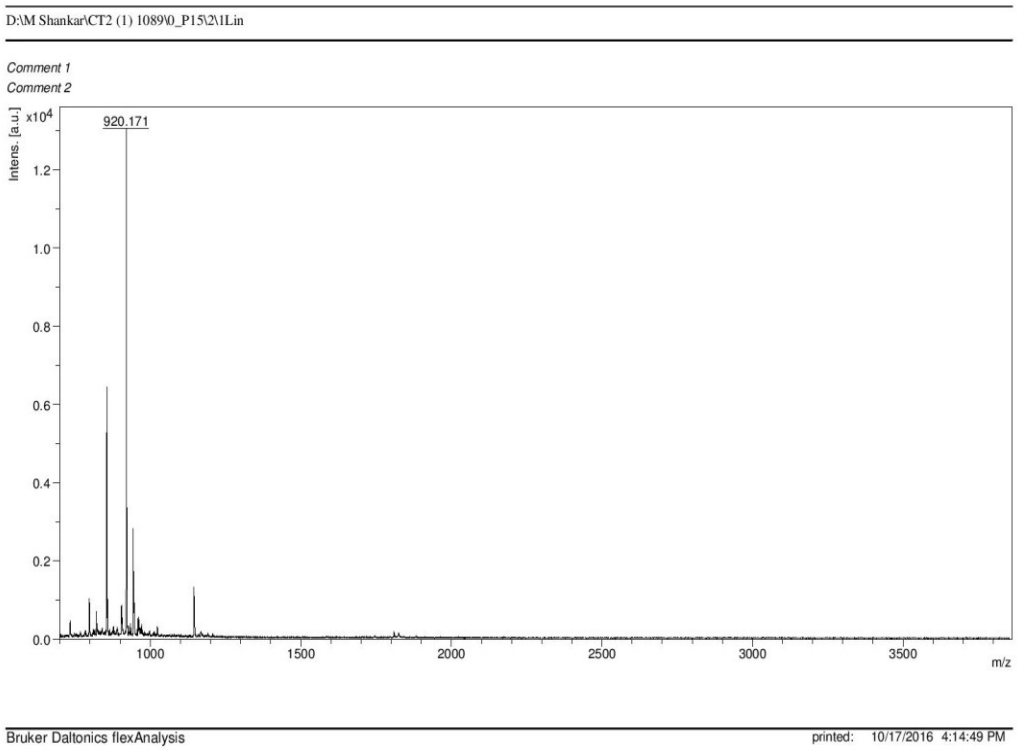

Figure S1. MALDI-TOF spectrum of **1** in CH_2Cl_2 using HABA matrix.

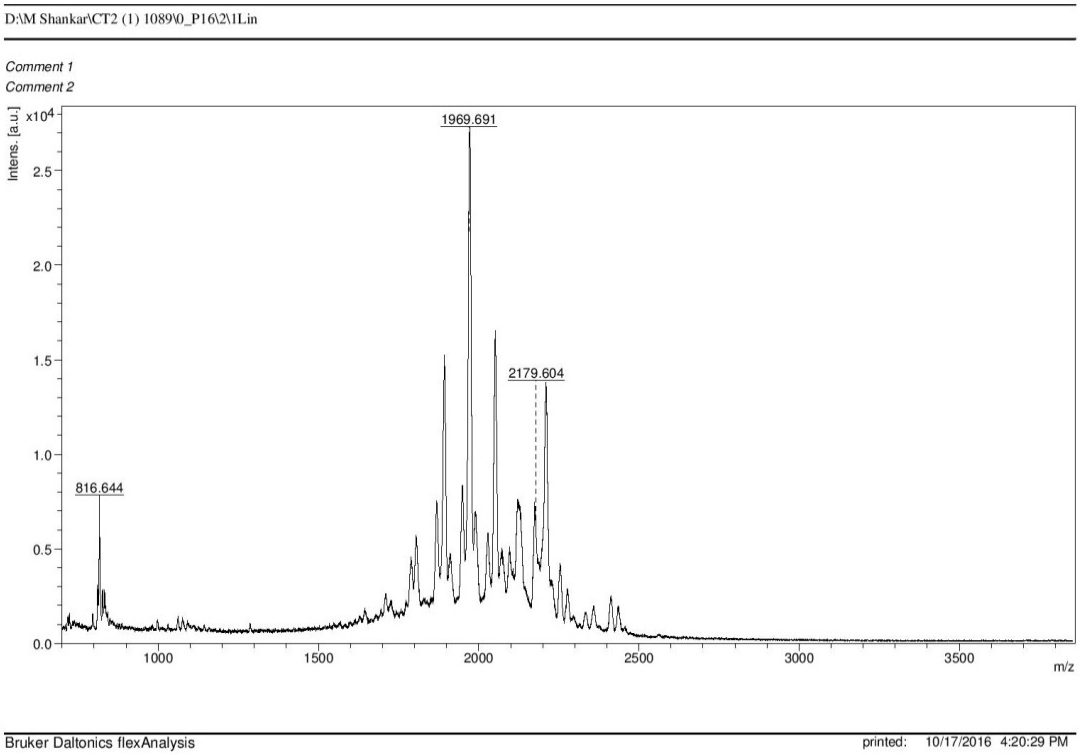

Figure S2. MALDI-TOF spectrum of **2** in CH_2Cl_2 using HABA matrix.

(a)

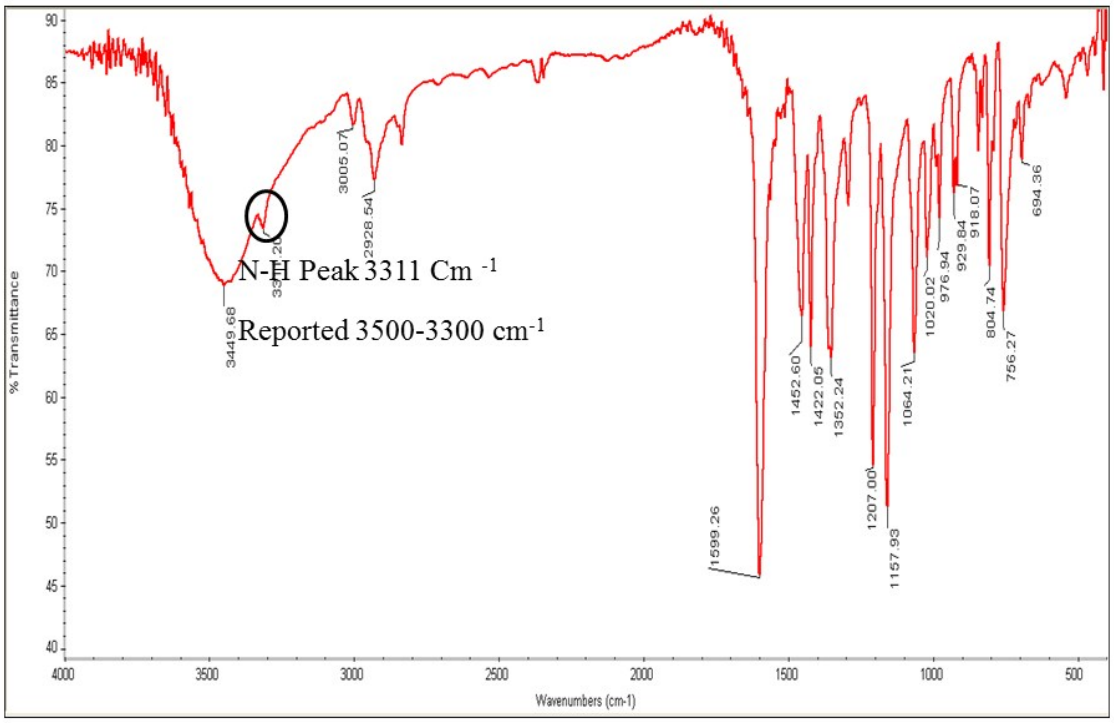
N-H Peak 3311 Cm -1
Reported 3500-3300 cm-1
% Transmittance
Wavenumbers (cm-1)
3449.68
3005.07
2928.54
1599.26
1452.60
1422.05
1352.24
1207.00
1157.93
1064.21
1020.02
976.94
929.84
918.07
804.74
756.27
694.36

(b)

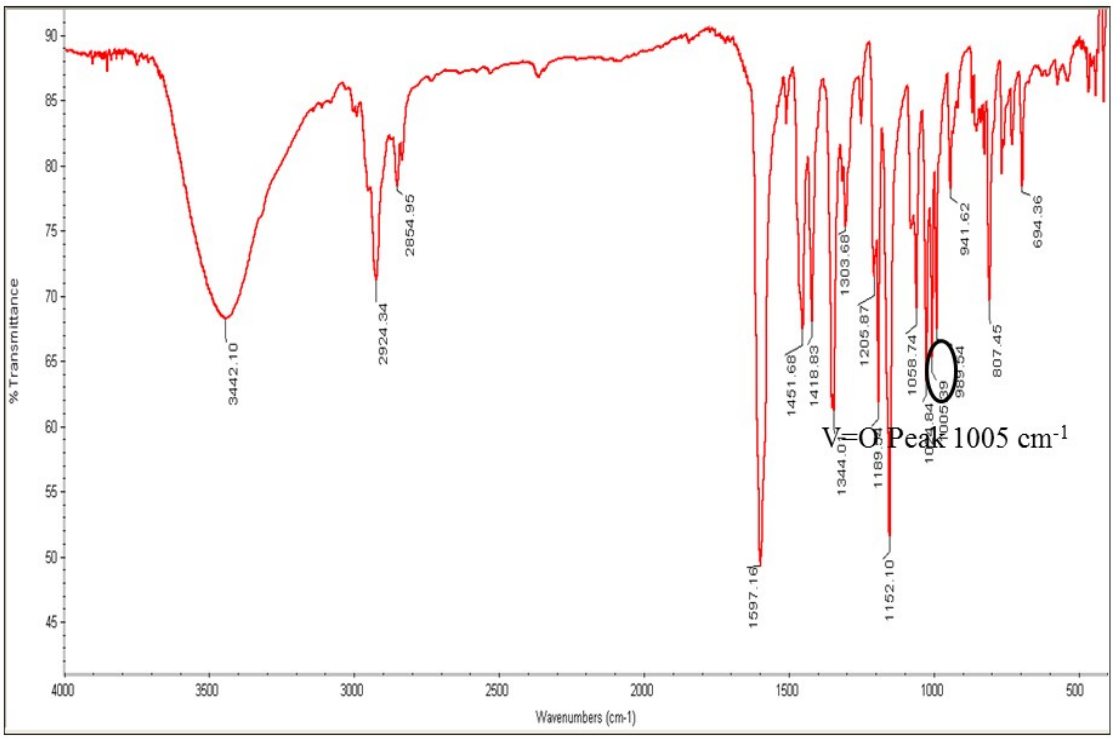
V=O Peak 1005 cm-1
% Transmittance
Wavenumbers (cm-1)
3442.10
2924.34
2854.95
1597.16
1451.68
1418.83
1344.01
1303.68
1205.87
1189.54
1152.10
1058.74
1005.99
989.54
941.62
807.45
694.36

(c)

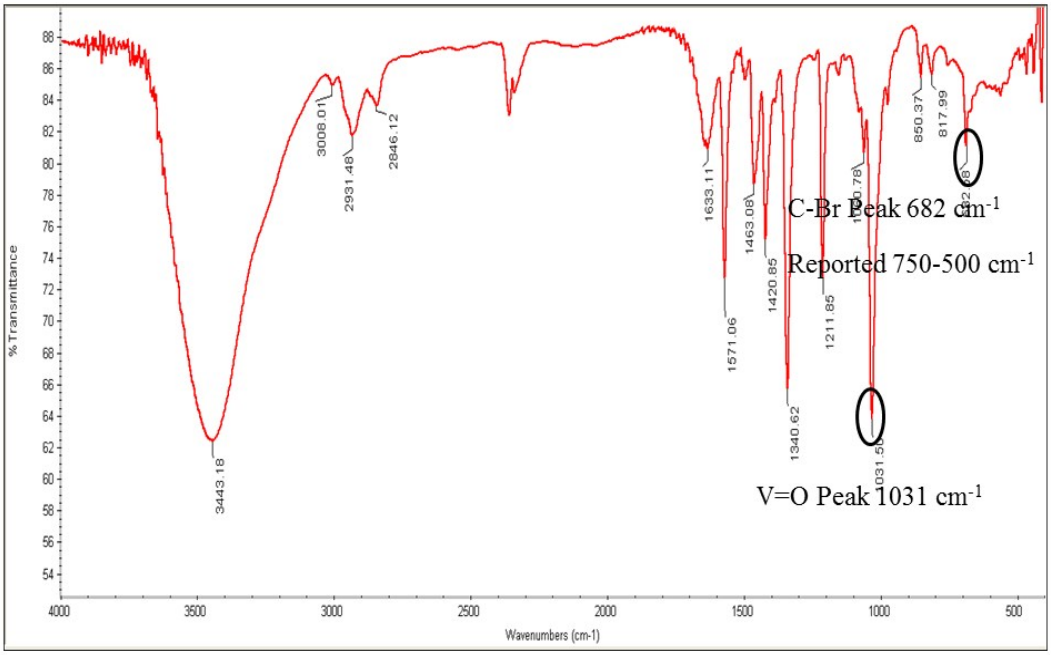

Figure S3. FT-IR spectra of (a) 3,5-dimethoxyphenyl porphyrin (b) **1** and (c) **2** using KBr pellets.

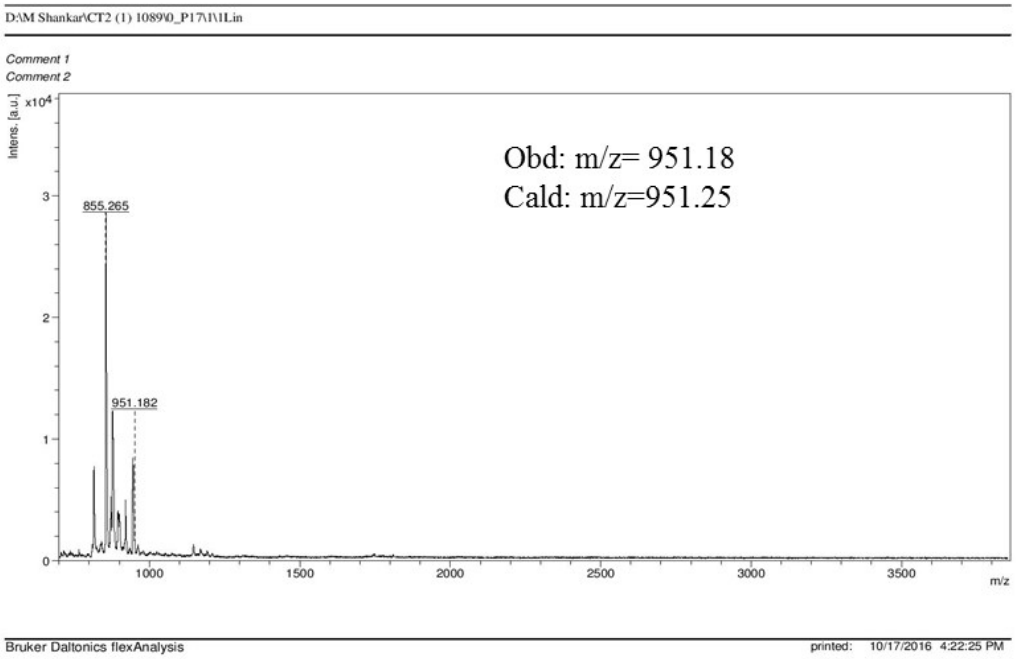

Figure S4. MALDI-TOF spectrum of oxidoperoxido species of **1** in CH_3CN generated with H_2O_2 and NaHCO3 using HABA matrix.

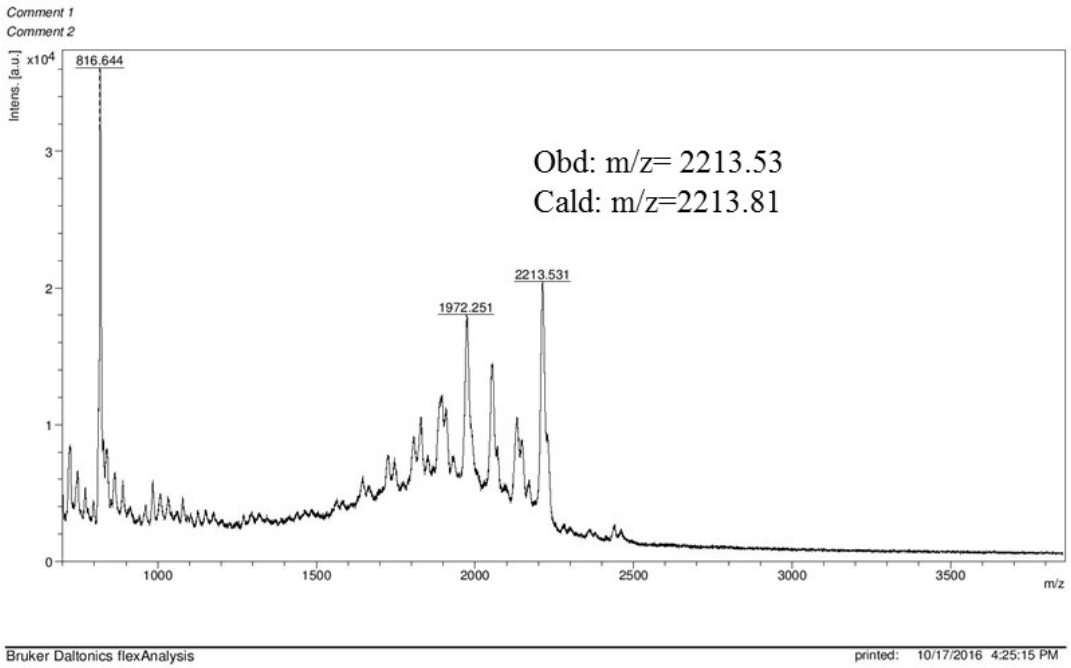

Figure S5. MALDI-TOF spectrum of oxidoperoxido species of **2** in CH_3CN generated with H_2O_2 and $NaHCO_3$ using HABA matrix.

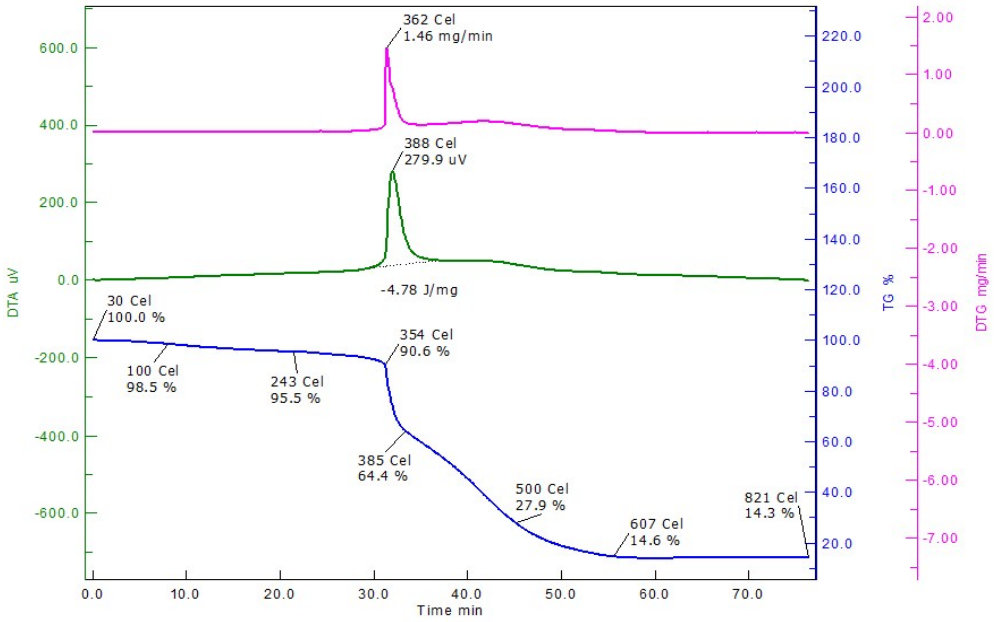

Figure S6. Thermogram (TG), Differential thermal analysis (DTA) and Differential thermogram (DTG) of 3,5-dimethoxyphenyl porphyrin, $H_2(TPP)(OMe)_8$ at a heating rate of 10 °C /minute scanned from 25 °C to 1000 °C.

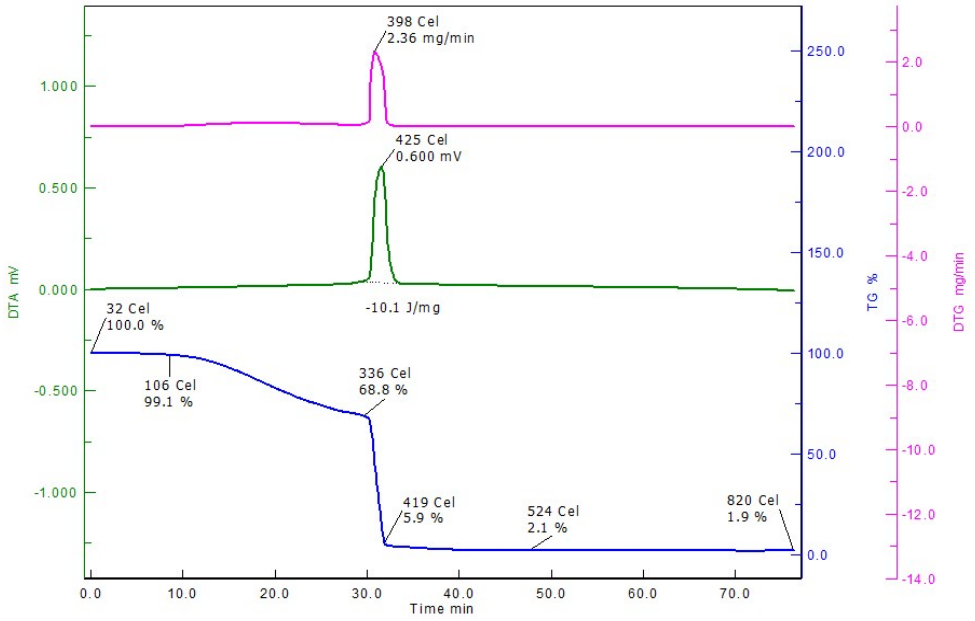

Figure S7. Thermogram (TG), Differential thermal analysis (DTA) and Differential thermogram (DTG) of (**1**) at a heating rate of 10 °C /minute scanned from 25 °C to 1000 °C.

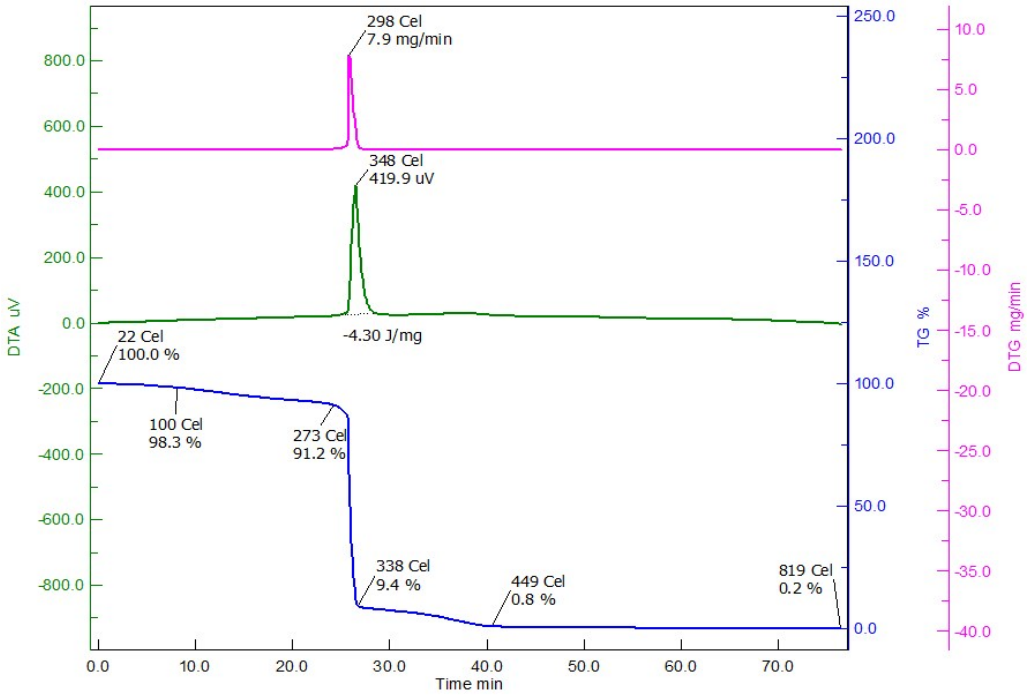

Figure S8. Thermogram (TG), Differential thermal analysis (DTA) and Differential thermogram (DTG) of (**2**) at a heating rate of 10 °C /minute scanned from 25 °C to 1000 °C.

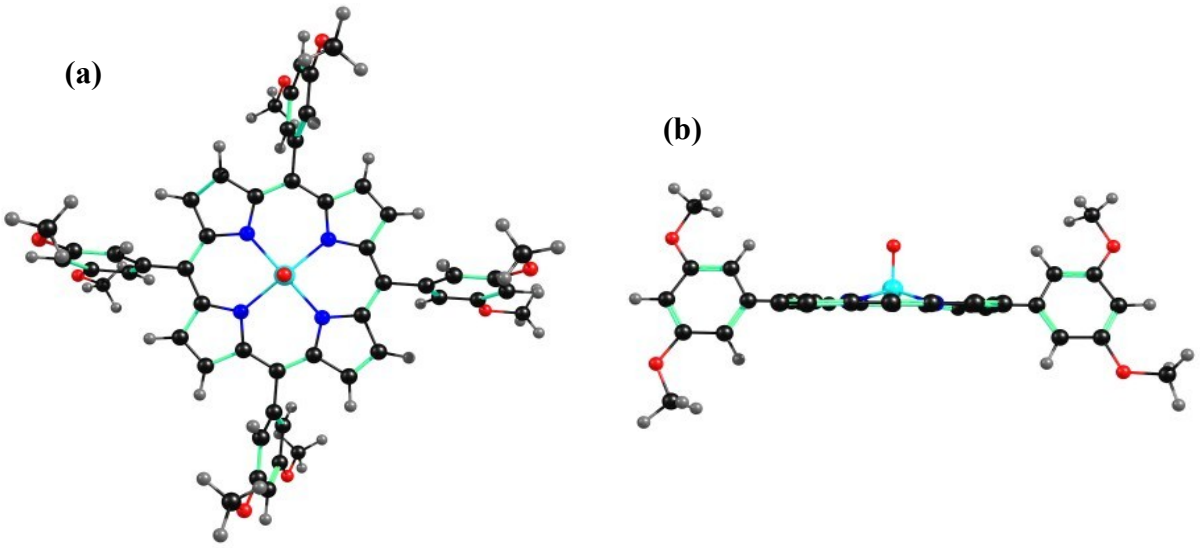

Figure S9. B3LYP/LANL2DZ set generated optimized geometry of **1** showing (a) top view and (b) side view. In the side view, front and back side substituents are not shown for better viewing.

Table S1. UV-Visible spectral data and molar absorptivity constants of **1** and **2** in CH_2Cl_2 at 298 K.

Compound	**B Band(s),nm**	**Q band(s), nm**
VO(TPP)$(OMe)_8$ (**1**)	425(5.57)	547(4.28)
VOT(TPP)(OMe)$(Br)_{16}$(**2**)	463(5.31)	592(4.24)

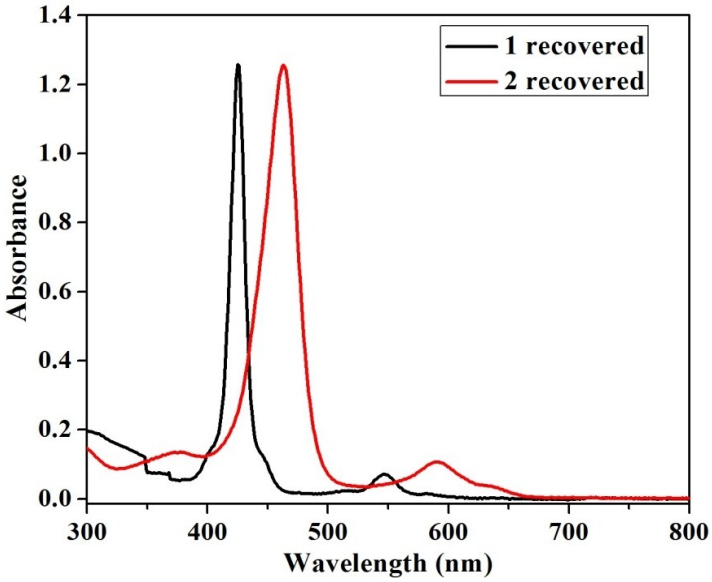

Figure S10. UV-Visible spectra of **1** and **2** after being recovered from the catalytic reactions in DCM at 298 K.

Table S2. Crystal structure data of VO(TPP)$(OMe)_8$ (**1**) and VO(TPP)$(OMe)_8(Br)_{16}$ (**2**).

	1-NC (from CH_3CN)	**2**
Empirical formula	$C_{53}H_{44}N_5O_9V$	$C_{52}H_{28}Br_{16}N_4O_9V$
Formula wt.	945.88	2182.28
Crystal system	Orthorhombic	Orthorhombic
Space group	P c c n	P c a b
a (Å)	13.829 (5)	20.733 (9)
b (Å)	14.439 (5)	26.304 (12)
c (Å)	26.153 (5)	28.112 (13)
α (˚)	90	90
β (˚)	90	90
γ (˚)	90	90
Volume (Å^3)	5222.15	15331.2
Z	8	12
D_{cald} (mg/m^3)	1.272	2.836
λ (Å)	0.71073	0.71073
T (˚C)	293 K	223 K
No. of total reflns.	6490	5640
No. of indepnt. reflns.	3816	2634
R	9.27	7.83
R_w	26.32	23.13
CCDC No.	1861934	1861933

Table S3. Selected average bond lengths and bond angles for $VO(TPP)(OMe)_8$ (**1**) and $VO(TPP)(OMe)_8(Br)_{16}$ (**2**) from single crystal XRD studies.

	1	**2**
Bond Length (Å)		
N-C_α	1.371 (9)	1.365 (4)
C_α-C_β	1.445 (1)	1.455 (5)
C_β-C_β	1.37 (1)	1.352 (5)
C_α-C_m	1.393 (1)	1.387 (5)
M-N	2.704	2.082 (3)
ΔC_β[a]	0.036	1.011
$\Delta 24$[b]	0.030	0.495
ΔC_α	0.026	0.396
ΔC_m	0.021	0.044
ΔN	0.033	0.113
ΔM	0.555	0.453
Bond Angle (°)		
N-C_α-C_m	125.725 (6)	124.262 (3)
N-C_α-C_β	110.02 (6)	106.875 (3)
C_β-C_α-C_m	124.26 (6)	128 (3)
C_α-C_β-C_β	107.03 (6)	107.625 (3)
C_α-N-C_α	105.92 (5)	110.242 (3)
M-N-C_α	126	121.875 (2)
N-M-N	150.955	154 (1)
adjacent pyrrole rings	2.96	35.065
Mean dihedral angle Relative to Mean Plane (°)		
meso-Ph	74.17, 75.43	55.6, 53.17
Pyrrole	1.41, 2.14	25.655, 24.695

[a]ΔC_β refers to the mean plane deviation of β-pyrrole carbons.

[b]$\Delta 24$ refers to the mean plane displacement of 24-atom core.

Equation 1: Equation used for calculating TOF

TOF (h^{-1}) = % conversion × mmol of substrate / 100 × mmol of cat. used × reaction time (h)